Geophysical Journal International

Geophys. J. Int. (2022) **230,** 565–579
Advance Access publication 2022 February 17
GJI Seismology

https://doi.org/10.1093/gji/ggac066

Central and Eastern European Infrasound Network: contribution to infrasound monitoring

István Bondár,[1] Tereza Šindelářová,[2] Daniela Ghica,[3] Ulrike Mitterbauer,[4] Alexander Liashchuk,[5] Jiří Baše,[2] Jaroslav Chum,[2] Csenge Czanik,[6,7] Constantin Ionescu,[3] Cristian Neagoe,[3] Marcell Pásztor[1,7] and Alexis Le Pichon[8]

[1] *Institute for Geological and Geochemical Research, Research Centre for Astronomy and Earth Sciences, Eötvös Loránd Research Network (ELKH), Budaörsi ut* 45, 1112 *Budapest, Hungary. E-mail: ibondar2014@gmail.com*
[2] *The Czech Academy of Sciences, Institute of Atmospheric Physics, Bočni II* 1401, 14100 *Prague* 4, *Czech Republic*
[3] *National Institute for Earth Physics (NIEP),* 12 *Calugareni St., PO Box MG-2,* 077125 *Magurele, Romania*
[4] *Zentralanstalt für Meteorologie und Geodynamik, Hohe Warte* 38, 1190 *Vienna, Austria*
[5] *Main Centre of Special Monitoring, National Center for Control and Testing of Space Facilities, State Agency of Ukraine, Moscovska, 8, Kyiv, 01010, Ukraine*
[6] *Institute of Earth Physics and Space Science, Eötvös Loránd Research Network (ELKH), Csatkai E. u. 6-8, Sopron, 6400, Hungary*
[7] *Department of Geophysics and Space Science, Institute of Geography and Earth Sciences, ELTE Eötvös Loránd University, Pázmány Péter sétány 1/C, 1117 Budapest, Hungary*
[8] *CEA/DAM/DIF, F-*91297, *Arpajon, France*

Accepted 2022 February 12. Received 2021 December 9; in original form 2021 October 5

SUMMARY

The Central and Eastern European Infrasound Network (CEEIN) has been established in 2018 with the collaboration of four research institutes, the Zentralanstalt für Meteorologie and Geodynamik (ZAMG), Vienna, Austria; the Institute of Atmospheric Physics of the Czech Academy of Sciences (CAS IAP), Prague, Czech Republic; the Research Centre for Astronomy and Earth Sciences of the Eötvös Loránd Research Network (ELKH CSFK), Budapest, Hungary; and the National Institute for Earth Physics (NIEP), Magurele, Romania. The Main Centre of Special Monitoring National Center for Control and Testing of Space Facilities, State Agency of Ukraine joined CEEIN in 2019. We show how the CEEIN infrasound arrays improve the detection capability of the European infrasound network and discuss coherent noise sources observed at CEEIN stations. We present the first CEEIN bulletin (2017–2020) of infrasound-only and seismo-acoustic events and using ground truth events, we demonstrate how adding infrasound observations to seismic data in the location algorithm improves location accuracy.

Key words: Seismic noise; Europe.

1 INTRODUCTION

The signature of the Comprehensive Nuclear-Test-Ban Treaty in 1996 and the deployment of the Comprehensive Nuclear-Test-Ban Treaty organization (CTBTO) International Monitoring System (IMS) infrasound component brought a renaissance to infrasound research (Marty 2019). Several studies estimated the detection capability of the IMS infrasound network (Le Pichon *et al.* 2009; Green and Bowers 2010), and Pilger *et al.* (2018) published the first European infrasound bulletin.

By the time the IMS infrasound network has reached near completion, infrasound networks supported by National means have also been deployed. For instance, beginning in the year 2010, every site in the US Transportable Array was equipped with an infrasound instrument (Trabant *et al.* 2012; IRIS DMC 2012; Walker *et al.* 2011). In Europe, the Atmospheric dynamics Research InfraStructure in Europe (ARISE, Blanc *et al.* 2018) project began focusing on the processes in the middle atmosphere (between altitudes 15 and 110 km) using infrasound, LIDAR and other technologies.

Established in 2018 as part of the ARISE2 network extension program (http://arise-project.eu), the Central and Eastern European Infrasound Network (CEEIN, Czanik *et al.* 2018; Šindelářová *et al.* 2018) laid the foundation for collaboration between four research institutes: (1) Zentralanstalt für Meteorologie and Geodynamik (ZAMG), Vienna, Austria; (2) Institute of Atmospheric Physics of the Czech Academy of Sciences (CAS IAP), Prague, Czech Republic; (3) Research Centre for Astronomy and Earth Sciences of the Eötvös Loránd Research Network (ELKH CSFK), Budapest, Hungary and (4) National Institute for Earth Physics (NIEP), Magurele, Romania. Seven microbarometer arrays were initially included in this regional network. In 2019, the network was extended to the East by Ukrainian infrasound stations, as the Main Centre of

Special Monitoring National Center for Control and Testing of Space Facilities, State Agency of Ukraine, joined CEEIN.

The main purpose of the CEEIN is to improve knowledge about infrasound in Central and Eastern Europe. As stipulated in the Memorandum of Understanding for the collaboration of the CEEIN, the main activities encouraged by the parties consist of: real-time data exchange of infrasound records inside and outside the group, production of the annual Central European Infrasound Bulletin, collaboration in scientific research such as infrasound propagation in local and regional distances, identification of infrasound sources, seismo-acoustic studies (Gibbons *et al.* 2019; Che *et al.* 2019) and discrimination between natural and anthropogenic events. Further information can be found at the CEEIN website, www.ceein.eu.

In this paper, we present the first CEEIN bulletin of infrasound-only and seismo-acoustic events, discuss sources of coherent noise, and show the improvements in detection capability of the European infrasound network due to CEEIN infrasound arrays. We also demonstrate improvements in location accuracy of seismo-acoustic events when adding infrasound observations to seismic data in the location algorithm.

2 DATA

Presently, CEEIN consists of 10 infrasound arrays of which nine are currently in operation. One of the arrays, I67RO in Romania deployed by NIEP in collaboration with CTBTO between 2016 and 2018 is no longer operational. The main characteristics of the CEEIN stations are summarized in Table 1.

The principal CEEIN arrays are ISCO, PVCI, PSZI, BURAR, IPLOR, I67RO, MAAG1, MAAG2 and GRDI. For ISCO, at first a mobile infrasound array was deployed together with seismic sensors to monitor the military training ground Allentsteig in Lower Austria. During one week a series of controlled explosions, originating from different sources, was recorded. ISCO operates permanently since 2021 January 04. The microbarograph array WBCI and the ionospheric Doppler sounder (IoDoSo, Chum *et al.* 2018) are included in CEEIN as complementary stations. Their main mission is observations of 3-D propagation of gravity waves at the ground and in the ionosphere/thermosphere. Besides, WBCI is used for monitoring low-frequency infrasound near the acoustic cut-off (0.0033–0.4 Hz) and IoDoSo is capable of monitoring infrasound in the ionosphere (Šindelářová *et al.* 2009).

IoDoSo measurements are based on the reflection of the radio waves from the ionosphere. If the ionospheric layer from which the radio wave reflects moves, for example, due to the interaction with acoustic gravity waves, then the reflected wave experiences a Doppler shift which provides information about the movement. A current configuration consists of five transmitters and two receivers. Thus, the points of reflection form a virtual array in the ionosphere suitable for propagation analysis of gravity waves in the ionosphere/thermosphere. IoDoSo operates on three radio wave frequencies, which means the sounding radio waves are reflected at different heights and vertical component of velocity of gravity waves and infrasound can also be estimated (Chum *et al.* 2021). Detailed explanations of the IoDoSo principles can be found in (Laštovička and Chum 2017).

Some of the CEEIN infrasound arrays are co-located with seismic stations, such as PSZI with the three-component broad-band PSZ station, BURAR and IPLOR with the BURAR and PLOR seismic arrays, respectively, MAAG1 with an auxiliary IMS seismic array AKASG, PVCI with the three-component broad-band PVCC station, and the WBCI array elements are co-located with STK, NKC, VAC and LBC seismic stations. Finally, ISCO is deployed in the premises of the Conrad observatory that accommodates a large underground installation covering the full geophysical monitoring program including seismology, gravity, meteorology and geomagnetism.

Infrasound waveform data are freely exchanged between CEEIN members in real and near-real time. PSZI data are available at the GEOFON EIDA node, the rest of the CEEIN waveforms are archived and accessible at the NIEP EIDA node. The CEEIN collaborative work increases the infrasound array coverage throughout Europe, and the data exchange and processing are of interest for civil applications in Central and Eastern Europe. Currently, five countries have already joined the CEEIN initiative, and we encourage further countries in the region to collaborate.

3 CEEIN BULLETIN 2017–2020

While the CEEIN infrasound arrays detect a plethora of various signals, we only include events in the CEEIN bulletin that can be located with an event location algorithm. We not only rely on CEEIN detections, but also collect seismic and infrasound data from other European local networks, the International Seismological Centre (ISC 2021) bulletin as well as detections from the IMS infrasound arrays.

We use iLoc, an open-source earthquake location algorithm to locate events (Bondár *et al.* 2018). iLoc is based on the ISC location algorithm (Bondár and McLaughlin 2009; Bondár and Storchak 2011), but has many additional features, such as the incorporation of the 3-D global upper-mantle velocity model, RSTT (Myers *et al.* 2010; Begnaud *et al*. 2021) and the use of arrival time, azimuth and slowness observations in event location.

Since the infrasound arrival time observations are less accurate than seismic arrival time measurements and the infrasound traveltime table is based on a 1-D velocity model that ignores seasonal variations, the infrasound arrival time observations are downweighted by the location algorithm. The *a priori* arrival time measurement error for infrasound arrival times is set to 8 s, 10 times larger than a first-arriving *P* phase. Thus, the contribution of infrasound arrival times is hundred times smaller than those of the first-arriving *P* phases in iLoc locations. On the other hand, infrasound backazimuth measurements are very accurate, for IMS-type arrays the uncertainty in back-azimuth measurements is on the order of 0.5° (Szuberla and Olson, 2004), therefore they are treated with the same data importance as first-arriving seismic *P* phases. Furthermore, for smaller aperture arrays the backazimuth uncertainty can be larger and it also increases with decreasing signal-to-noise ratio. Because of this and the fact that backazimuth measurements are not wind-corrected, iLoc assumes a conservative *a priori* backazimuth measurement error of 1.0°, twice as much as larger measurement errors in the azimuth determination than one would use if the wind effects were taken into account. Considering wind effects in a routine operational environment would require near real time access to atmospheric models to perform ray tracing, which would hamper the performance and speed of the system. One of the strengths of iLoc is that it can be used in real time processing, especially now that it is implemented in SeisComp (Weber *et al.* 2019; https://docs.gempa.de/seiscomp/current/index.html). Thus, especially when combined with seismic observations, it can give fast and reliable locations for seismo-acoustic events that can be used as starting points in more involved studies.

Table 1. CEEIN stations.

Station	Country	Latitude	Longitude	No. of sensors	Type of sensors	Aperture (km)	Operation period From	Operation period To
ISCO	Austria	48.73	15.57	4	Hyperion IFS-3000	0.36	2020/10/30	2020/11/06
		47.93	15.87			1.11	2021/01/04	Now
PVCI	Czechia	50.53	14.57	3	The Scientific and Technical Centre 'Geophysical Measurements' ISGM03	0.20	2014/05/01	Now
WBCI		50.25	12.44	4	Paroscientific 6000-16 B-IS	6.00	2016/09/28	Now
PSZI	Hungary	47.92	19.89	4	SeismoWave MB3d	0.25	2017/05/25	Now
BURAR	Romania	47.62	25.22	4	Chaparral Physics Model 21	0.60	2016/07/28	2019/09/20
		47.62	25.22	6	Hyperion IFS-5113	0.69	21/09/2019	Now
IPLOR		45.85	26.65	6	Chaparral Physics Model 25	2.43	2009/05/28	2018/11/09
				4		0.49	2019/12/13	Now
I67RO		46.67	23.12	4	SeismoWave MB2005	0.95	2016/09/27	2018/10/18
MAAG1	Ukraine	50.70	29.23	3	Broadband microbarometers K-304	0.16	09/2006	Now
MAAG2		48.56	26.46	4		0.16	05/2007	Now
GRDI		50.60	29.45	4	DI digital sensor	0.40	07/2020	Now

Table 2. Events by type in the CEEIN bulletin.

Event type	**Number of events**	Number of ground truth events
Earthquakes	2	0
Bolides	3	0
Sonic booms	23	0
Explosions	24	24
Quarry blasts	4	4

We included events in the CEEIN bulletin that were recorded by at least two CEEIN infrasound arrays. The Supporting Information contains the first CEEIN bulletin for the period 2017–2020. Table 2 shows the summary of events in the CEEIN bulletin that list the number of events by their source type.

The bolide over the Slovenian-Croatian border on 2020 February 28 as well as the quarry blasts in Austria and Romania are located by only the CEEIN infrasound arrays and local seismic stations. There are many more quarry blasts and explosions that are recorded in our region by a single CEEIN array, but because of their very local nature we did not include them in the CEEIN bulletin. Furthermore, the explosions and quarry blasts are ground truth events, that could help validating atmospheric models and ray tracing algorithms. Note that we consider an event ground truth only if its location is known at a high confidence.

Fig. 1 shows the location of the events in the CEEIN bulletin. CEEIN stations (yellow symbols) as well as ground truth events (green stars) that are discussed in the text are labelled in the map.

Some of the events in the bulletin, such as the ammunition storage explosions Kalynivka and Ichnya, the Ingolstadt oil refinery explosion, the Beirut explosion and quarry blasts in Austria and Romania qualify as ground truth, because we know exactly where and when they occurred.

The bolides in the bulletin are infrasound-only locations. The fireball near Lipetsk, Russia in 2018 (Varypaev *et al.* 2019), was observed by seventeen infrasound stations, seven of which belong to CEEIN. However, only two of the CEEIN stations, BURAR and MAAG2 detected the distant fireball over the Bering Sea in 2019 (59.34°N, 176.21°E, not shown on the map). Nevertheless, the event was well recorded by the IMS network.

Infrasound signals generated by the bolide above the Croatian–Slovenian border in 2020 were detected by seismic stations. The fireball was also observed by CEEIN stations PSZI, BURAR, IPLOR, MAAG2, while only I26DE from the IMS infrasound network recorded the event. Similarly, mostly seismic stations recorded the infrasound signals from the Baumgarten, Austria explosions (Schneider *et al.* 2018). Although PSZI has arguably detected the Baumgarten explosion (Koch *et al.* 2020) we did not include the event, because no other CEEIN stations reported it; at the time the Austrian array was not operational.

4 CEEIN DETECTION CAPABILITY

The employment of the CEEIN stations improved the ability to identify infrasound sources in Central and Eastern Europe. The region has so far been rather marginalized as regards infrasound

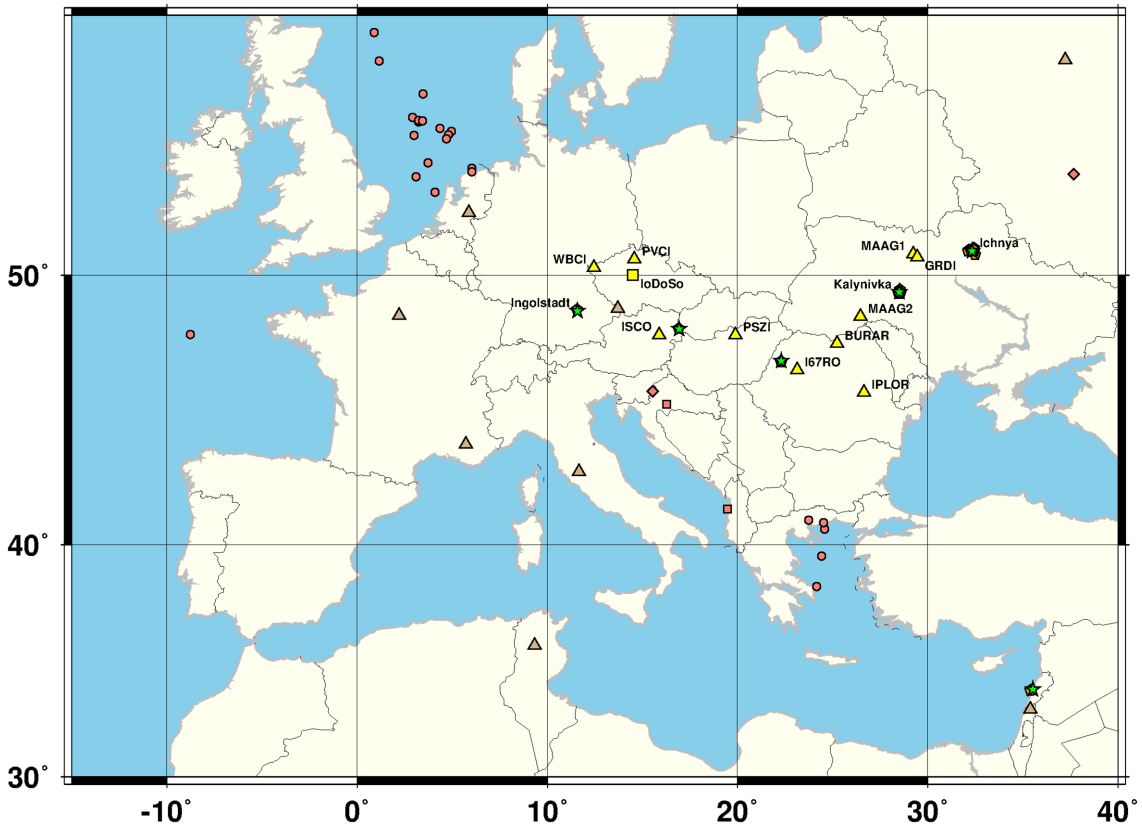

Figure 1. Events in the CEEIN bulletin, 2017–2020. Yellow triangles indicate CEEIN infrasound arrays, the yellow square represents the ionospheric Doppler sounder. IMS and other infrasound arrays are shown as tan triangles. Red circles indicate sonic booms over the North Sea and Aegean Sea, red pentagons mark explosions and quarry blasts, red squares denote earthquakes and red diamonds indicate bolides. Green stars mark the ground truth locations of the explosions. Events that are discussed in the text are labelled by their names.

research. Before the deployment of CEEIN arrays, only two IMS stations, I26DE and I43RU offered infrasound station coverage for the region.

Using the method introduced by Le Pichon *et al.* (2012), the detection capability maps were generated and detection capabilities were compared of the infrasound network that involves CEEIN stations against the network without CEEIN stations. The frequency-dependent attenuation relations are derived from a huge number of numerical simulations based on the wide-angle Parabolic Equation method (Collins 1993; Gainville *et al.* 2010; Green *et al.* 2011). The model includes effects of geometrical spreading and attenuation (Sutherland and Bass 2004); it also takes fine-scale atmospheric structures into account. The parameters of the stratospheric winds on the given day of the year are obtained from the models provided by the European Center for Medium range Weather Forecasting (www.ecmwf.int). The detection capability simulations account for the combined effects of the signal frequency, stratospheric wind and fine scale atmospheric disturbances which influence long-range infrasound propagation (Le Pichon *et al.* 2012). From the attenuation curves, detection thresholds are derived from reference station noise models (Brown *et al.* 2014). The simulations of the detection capabilities of the global IMS infrasound network showed that below 0.8 Hz the signal attenuation is nearly constant during the year, but the attenuation is seasonal dependent at higher frequencies. Near equinoxes the increase of signal attenuation was observed above 1.6 Hz (Le Pichon *et al.* 2012). The detection capabilities of the infrasound network with and without CEEIN stations were therefore modelled for these two threshold frequencies of 0.8 and 1.6 Hz.

The detection capabilities were modelled for the year 2019. To obtain the maximum possible detection capability of the network, the simulation includes all of the permanent CEEIN stations—CEEIN stations in operation as well as stations under construction in 2019 (see Table 1 for details). Fig. 2 shows the differences between the detection capability of the infrasound network without the CEEIN stations and the detection capability of the network with all the permanent CEEIN stations involved on March 20, June 22, September 23 and December 17, four days representing four seasons of the year. Fig. 2 also shows the detection capabilities in periods influenced by sudden stratospheric warmings (SSW) for 2017 February 01 and for 2018 February 15.

The involvement of the CEEIN stations in infrasound detections improves the performance of the network in central and eastern Europe in all seasons of the year. CEEIN decreases the minimum detectable source amplitude and helps identifying weaker infrasound sources and facilitates more accurate localizations. The CEEIN stations contribute to infrasound detections particularly in the region approximately delimited with 25–55°N and 15–35°E. A rather western localization of the region prevails in winter. In summer, the maximum improvement of the detection capability shifts to the East to longitudes between 25° and 35°E. We point out the better coverage of the Eastern Mediterranean and of the Black Sea in summer when CEEIN stations are involved in detections. The network without CEEIN stations was only able to detect sources of minimum amplitudes of 30–40 Pa located in the mentioned regions on 2019 June 22. The minimum detectable source amplitude (at a reference distance of 1 km) decreases by more than 10 Pa in the

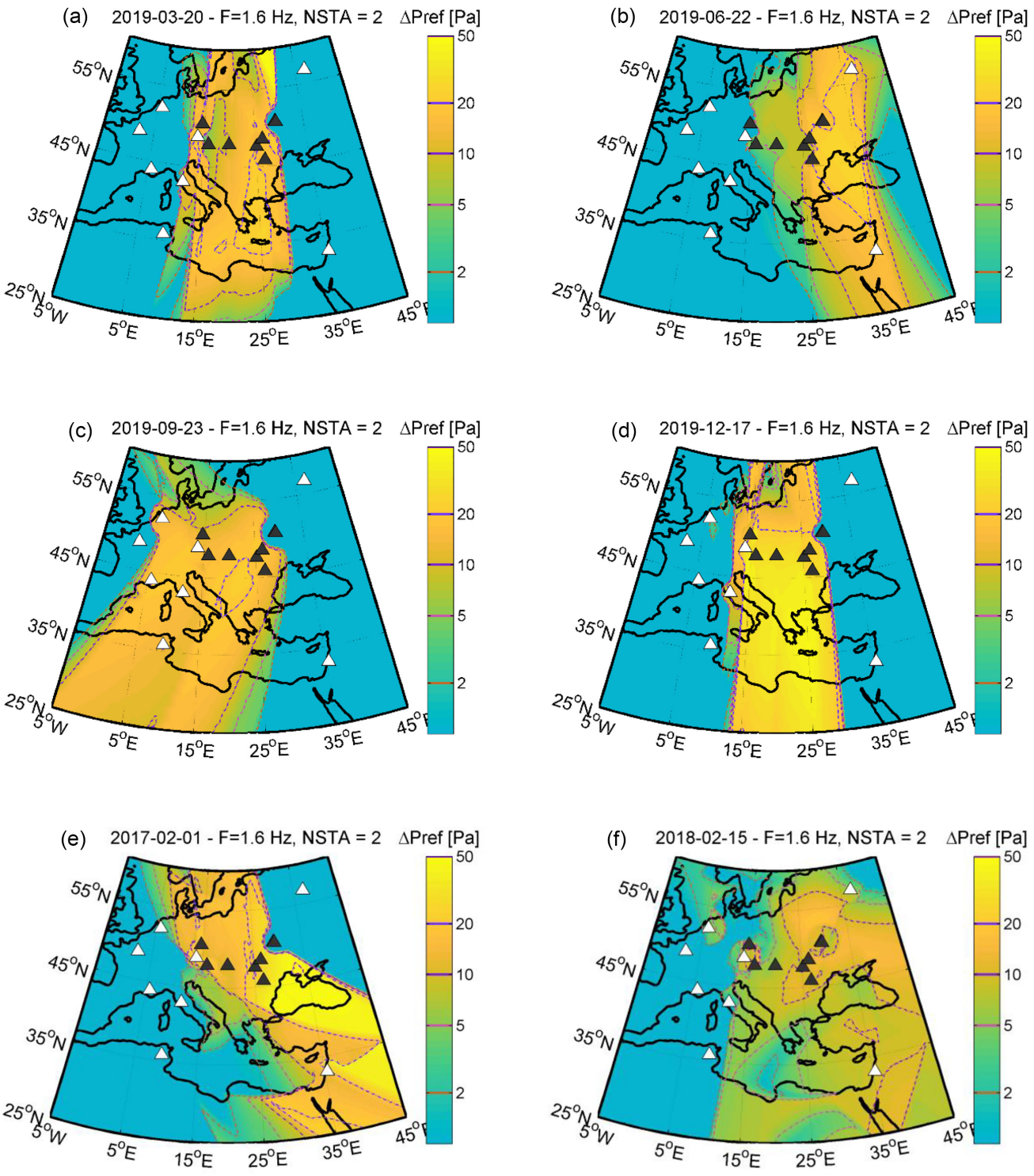

Figure 2. Difference between the detection thresholds of the infrasound network in Europe with the CEEIN stations included and without the CEEIN stations. The colour scale indicates the difference (with respect to a reference distance of 1 km from the source, in Pascal); yellow means large improvement of the detection capability and blue means no difference between the detection capabilities of the network with and without CEEIN. The detection capabilities were modelled at 1.6 Hz. At least two stations are required to detect a signal arriving from a given location. The CEEIN stations are represented with grey triangles; other infrasound stations (IMS and national arrays) are indicated as white triangles. (a) 2019 March 20, (b) 2019 June 22, (c) 2019 September 23, (d) 2019 December 17, (e) 2017 February 01 and (f) 2018 February 15.

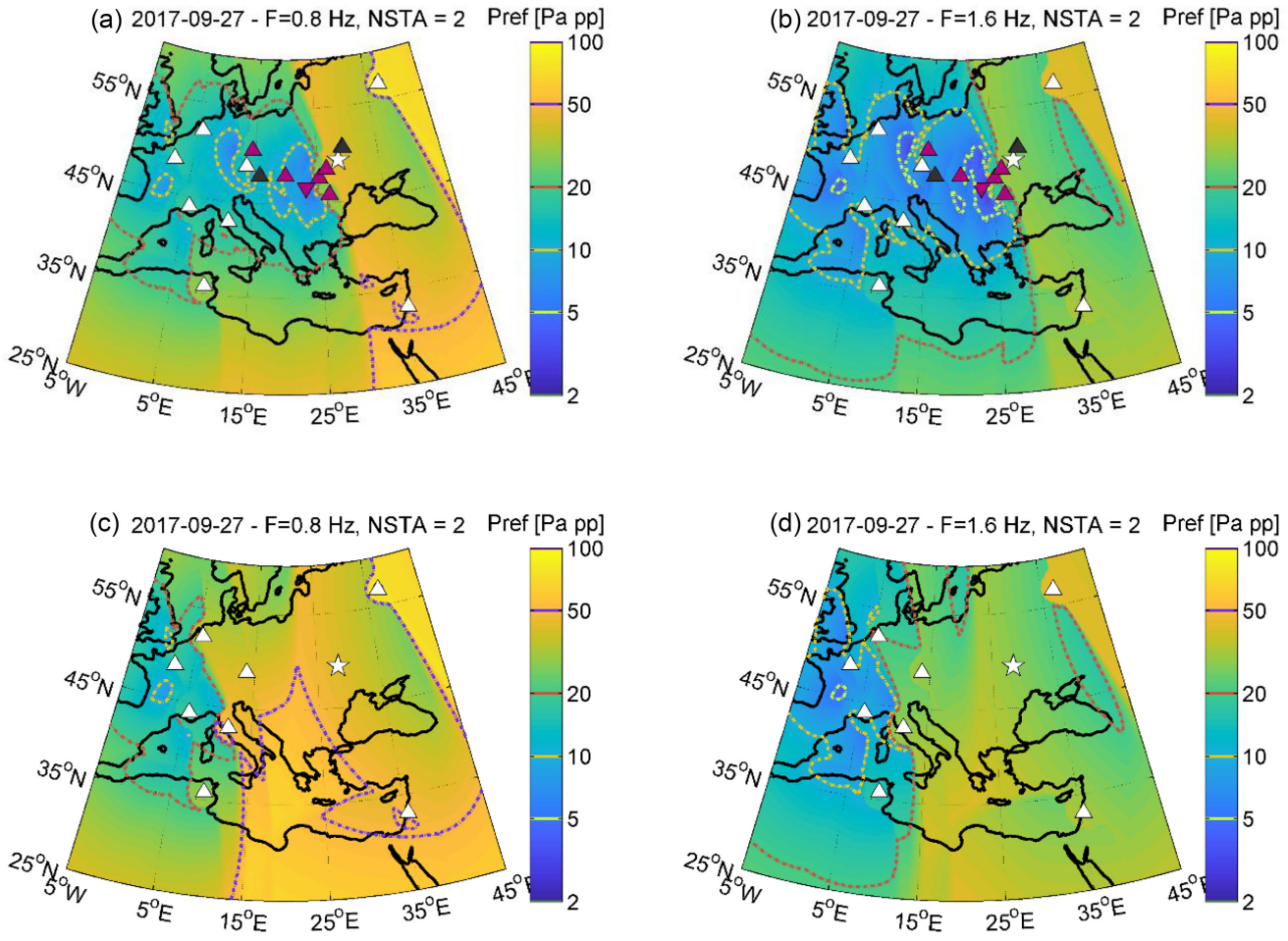

Figure 3. Detection capability *with* the CEEIN stations on 2017 September 27, (a) at 0.8 Hz and (b) at 1.6 Hz. Detection capability *without* the CEEIN stations (c) at 0.8 Hz and (d) at 1.6 Hz. The CEEIN stations in operation on 2017 September 27 are represented with red triangles, the CEEIN stations under construction are represented with grey triangles; the temporary deployed station I67RO is distinguished with an inverted triangle. IMS and other national infrasound stations are shown as white triangles. The explosion site Kalynivka is marked with a white star.

Eastern Mediterranean and by about 20 Pa in the Black Sea region once CEEIN is added in the infrasound network.

In winter, when the stratospheric waveguide is driven by westerly stratospheric winds, sources located west of infrasound arrays are detected. CEEIN stations in Eastern Europe fill in the spatial gap and enable observations of sources in Central Europe. Whereas the network without CEEIN was able to detect only strong sources of amplitudes larger than 30 Pa in central Europe and of amplitudes larger than 50 Pa in central Mediterranean on 2019 December 17, the network with the CEEIN stations enabled observations of source amplitudes below 20 Pa in central Mediterranean. The detection capability in Central Europe improved so that source amplitudes around 10 Pa were detectable and the detection threshold dropped down to 5 Pa in limited regions particularly in eastern Europe. Extraordinary winter conditions for infrasound propagation could form during SSWs (e.g. Evers *et al.* 2012; Assink *et al.* 2014) such as those in that occurred in 2017 and 2018 February. The changes of the stratospheric circulation are reflected in the detection capability maps (Figs 2e and f). During the SSWs, CEEIN stations improve coverage in eastern Europe and in eastern Mediterranean, which corresponds to usual network performance in summer.

Near equinoxes when the stratospheric waveguide gets weak due to the seasonal reversal of zonal stratospheric winds and the remote monitoring of the events is reduced, observations by local stations become increasingly important. The improvement of detection capabilities is obvious in panels (a) and (c) in Fig. 2. Better network performance is predicted particularly in Central Europe and in the Mediterranean on 2019 March 20 and September 23; the difference between detection capability of the network with and without CEEIN reaches up to 20 Pa. It holds particularly for frequencies higher than 0.8 Hz where atmospheric absorption of infrasound increases in the thermospheric waveguide (Le Pichon *et al.* 2012; Sutherland and Bass 2004). On 2019 March 20, the detection capability of sources located in Central Europe improved from detection thresholds of 20–30 Pa to values around 10 Pa. Similar detection thresholds were obtained on 2019 September 23.

Based on the seasonal regime of zonal stratospheric winds we define spring from March 1 to April 30, summer from May 1 to August 31, autumn from September 1 to October 31 and winter from November 1 to February 28 for the purposes of our study. We presented four cases that represent the most typical picture of the CEEIN contribution to the infrasound detection capabilities in a given season of the year. Deviations from these values and spatial coverages can occur particularly when winter stratospheric dynamics is influenced by SSWs. On the other winter days and also in summer the contribution of CEEIN to the detection capabilities seems

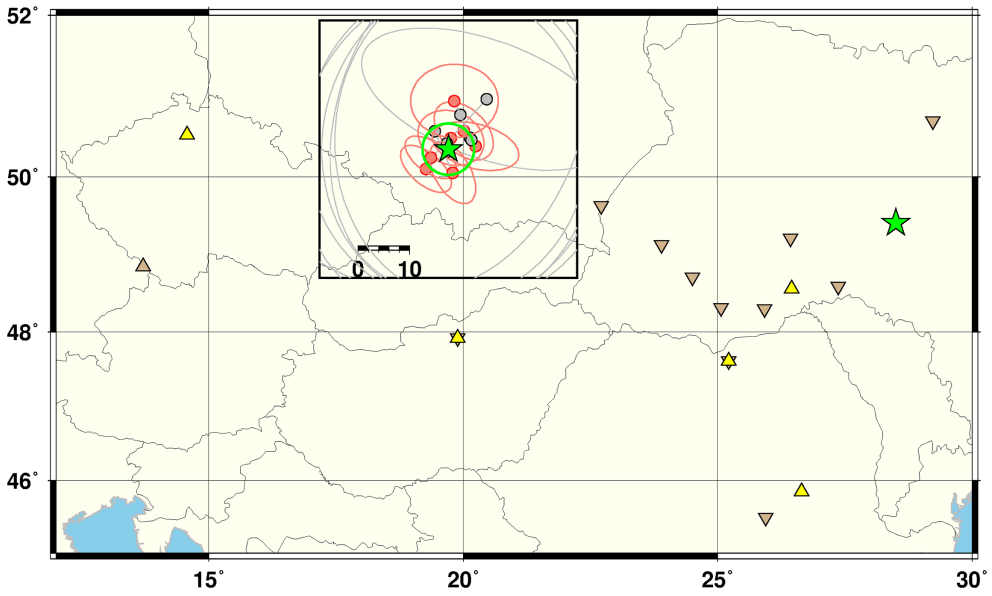

Figure 4. Event locations for Kalynivka, Ukraine. Inverted triangles mark the seismic stations, yellow and beige triangles indicate CEEIN and IMS infrasound arrays that recorded the events. Green star indicates the ground truth location. The inset shows the enlarged vicinity of the ground truth locations. Red and grey circles indicate the CEEIN and IDC solutions, and grey and red lines show the corresponding error ellipses, respectively. The green circle is the 5 km radius around the GT site.

stable and the minimum detectable source amplitude decreases by 10–30 Pa in summer and by 10–50 Pa in winter. The detection capability maps show larger variability in the spring and autumn transition periods when the efficiency of the stratospheric waveguide decreases due to the seasonal reversal of zonal stratospheric winds. For example, in 2019 September, we could observe transition from summer type of detection capabilities that still persisted on September 1–13 to the autumn type that appeared on September 22. On September 16, the detection thresholds were between 20–30 Pa of the source amplitude in Central and Eastern Europe, involvement of CEEIN could only improve detection capabilities in limited regions close to the CEEIN stations.

4.1 Selected ground truth events

The detection capability of the infrasound network with and without CEEIN stations is compared for selected ground truth events. Only those of the CEEIN stations that were in operation during the respective events are involved in the simulations, these are shown in the detection capability figures as red triangles. Detection capability is modelled for signals with 0.8 and 1.6 Hz dominant frequencies. We require at least two stations to detect signals arriving from the source. The colour scale in Figs 3, 5 and 6 represents the minimum detectable amplitude of the signal.

4.1.1 Ammunition depot explosions in Kalynivka, Ukraine, 2017 September 26–27

The infrasound network, as well as a local seismic network recorded a series of explosions in the ammunition depot in Kalynivka, Ukraine between 2017 September 26, 19:02 UTC and 2017 September 27, 05:09 UTC. The events occurred near autumn equinox, that is, in the period of the year when a decreased effectiveness of the stratospheric waveguide is expected. Therefore, the minimum detectable signal amplitude from a source in the region of the Kalynivka explosions remains similar regardless whether CEEIN is involved in detections or not, as the comparisons between panels (a) and (c) and panels (b) and (d) show. Nevertheless, the shock waves originating from an explosive source such as the Kalynivka series of explosion would always exceed the relatively high values of minimum detectable amplitudes of 20–50 Pa.

Fig. 4 shows the event locations in the CEEIN bulletin. All of the seven reported explosions were recorded by the CEEIN stations MAAG2, BURAR, IPLOR and PSZI. PVCI, the most distant CEEIN station from the explosion epicentre (∼1000 km), observed only two explosions. It can be assumed that the above discussed decreased efficiency of the stratospheric waveguide influenced observation at PVCI. Though of the two closest stations MAAG1 was under repair and GRDI has not yet been deployed at the time of the events, the contribution of CEEIN is obvious. The inset in Fig. 4 represents the immediate vicinity of the ground truth site, showing the individual IDC and CEEIN locations, respectively. The inclusion of CEEIN stations and local seismic network significantly reduces the size of the error ellipses.

4.1.2 Oil refinery explosion in Ingolstadt, Germany, 2018 September 01

The oil refinery explosion in Ingolstadt, Germany on 2018 September 01 at 03:11 UTC was another autumn equinox event (Fuchs *et al.* 2019; Koch and Pilger 2020). The explosion was registered by the CEEIN stations PVCI, PSZI, IPLOR, BURARI and I67RO. The CEEIN stations did not noticeably improve the network detection capability for this event (Fig. 5), because the source region was well covered by the IMS station I26DE and also the national arrays in France, Germany, and Italy that had the potential to observe the explosion.

Nevertheless, the Ingolstadt explosion cannot be located by the sparse IMS infrasound network alone as only I26DE detected the event.

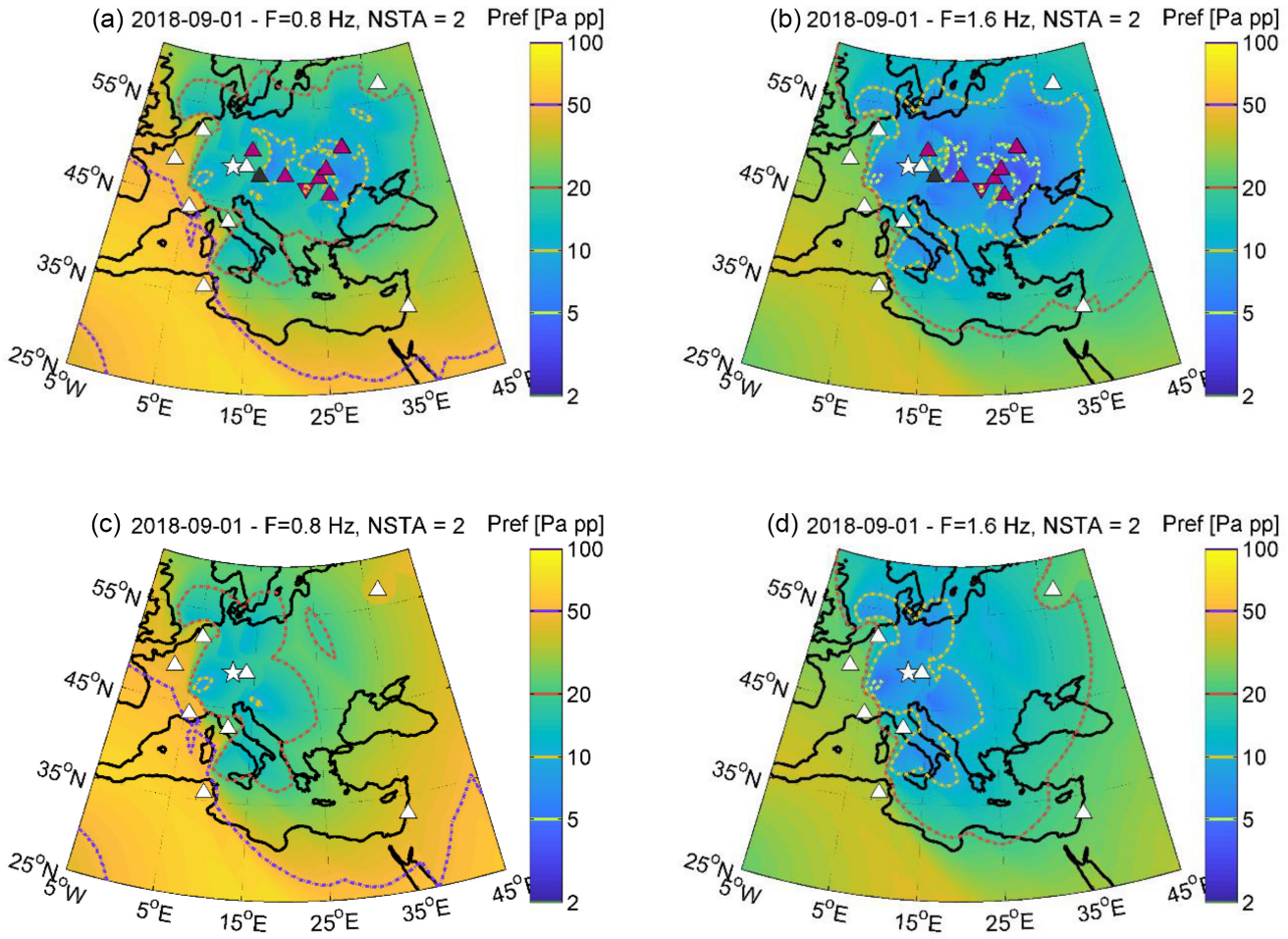

Figure 5. Detection capability *with* the CEEIN stations on 2018 September 01, (a) at 0.8 Hz and (b) at 1.6 Hz. Detection capability *without* the CEEIN stations (c) at 0.8 Hz and (d) at 1.6 Hz. The CEEIN stations in operation on 2018 September 01 are represented with red triangles, the CEEIN stations under construction are represented with grey triangles; and the temporary deployed station I67RO is distinguished with an inverted triangle. IMS and other national infrasound stations are shown as white triangles. The explosion site Ingolstadt is marked with a white star.

4.1.3 Ammunition depot explosions in Ichnya, Ukraine, 2018 October 10

A series of explosions at the military warehouse Ichnya, Ukraine occurred in early 2018 October. The stratospheric waveguide in this part of the year is getting under the influence of westerly winds and as a consequence signal propagation to the east from its source is supported. The chance to observe the Ichnya explosions at western European stations was thus limited as predicted by the detection capability model. Fig. 6 shows the detection capability of the European infrasound network without and with the CEEIN stations.

Indeed, from the IMS network only the eastern stations, I31KZ, I43RU and I46RU recorded the events. MAAG1 and IPLOR detected all of the fourteen reported explosions. BURAR was able to register four explosions, although the stations are located to the west from the explosion site. Despite the fact that the CEEIN station are also located to the west of the events, they could benefit from a significantly shorter distance from the explosion site than the closest IMS station I26DE to the West (230 km distance of MAAG1, but 1360 km distance of I26DE). Fig. 7 shows the event locations in the CEEIN bulletin. As in the case of the Kalynivka explosions, the inclusion of CEEIN observations not only improve location accuracy but also reduce location uncertainty as the error ellipses invariably get smaller with CEEIN data. The reduction in the size of error ellipses is attributed to the fact that the inclusion of CEEIN and seismic data increase number of observations that can be used in the location that results in more precise uncertainty estimates.

Together with the above discussed events, the series of ammunition storage explosions in Ichnya is a good demonstration of the importance of the CEEIN for monitoring of infrasound events in Europe and shows that the CEEIN suitably completes the well-established ARISE infrasound network.

Fig. 8 shows the histogram and cumulative distributions of the distance from ground truth events of the IDC and the CEEIN solution. Both the IDC locator and iLoc can use seismic, hydroacoustic and infrasound arrival time, slowness and backazimuth measurements and both scale the error ellipse to the 90 per cent confidence level. Therefore, the IDC and iLoc solutions are comparable, the only difference being the inclusion of CEEIN data in the locations. Adding CEEIN stations increases the number of observations that can be used in the location, thus allowing more precise location estimates reflected in the reduction of the size of error ellipses. As Fig. 8 demonstrates, CEEIN stations also improve location accuracy by reducing the mislocation of the ground truth events.

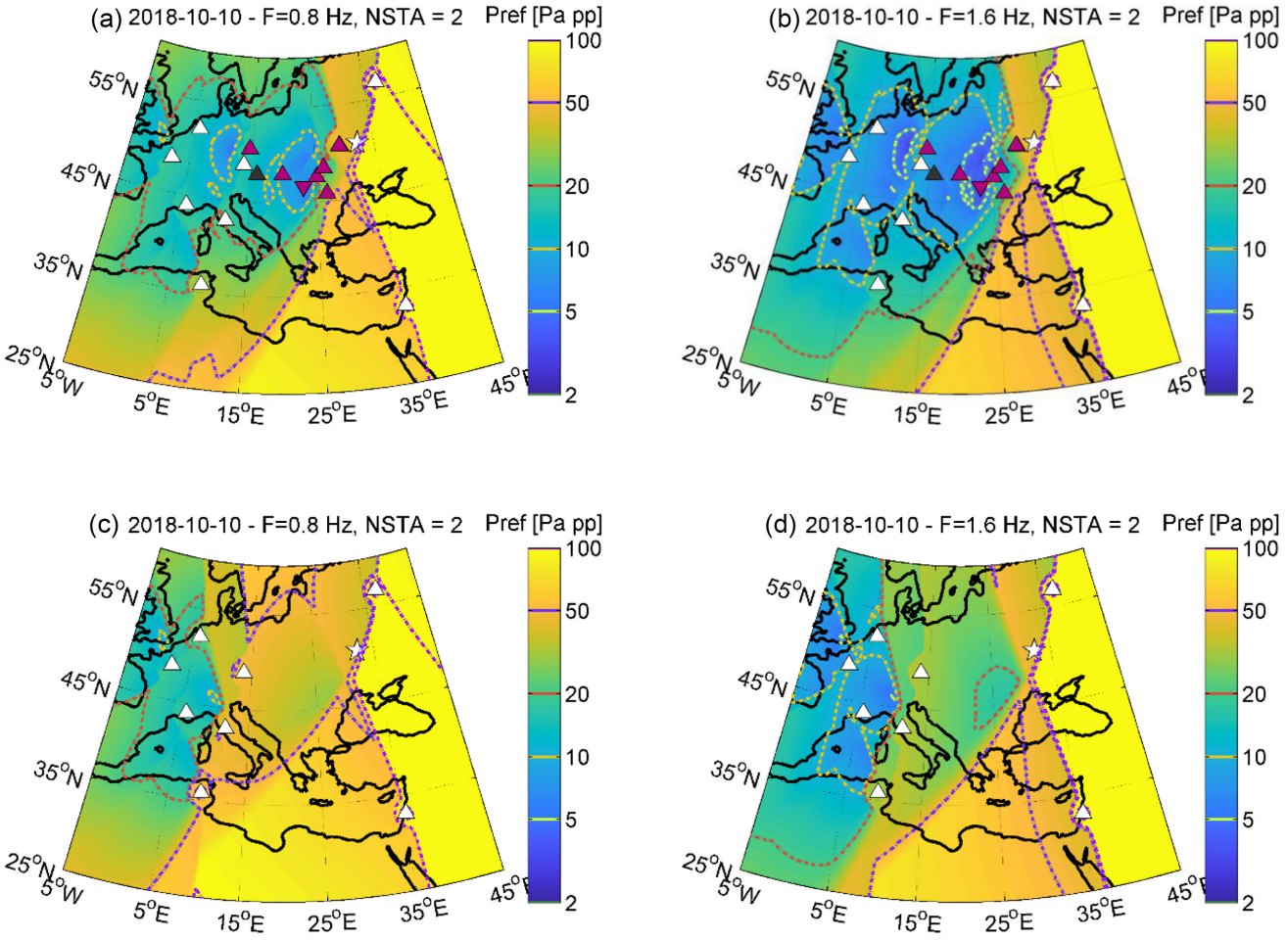

Figure 6. Detection capability *with* the CEEIN stations on 2018 October 10 (a) at 0.8 Hz and (b) at 1.6 Hz and *without* the CEEIN stations (c) at 0.8 Hz and (d) at 1.6 Hz. The CEEIN stations in operation on 2018 October 10 are represented with red triangles, the CEEIN stations under construction are represented with grey triangles; and the temporary deployed station I67RO is distinguished with an inverted triangle. IMS and other national infrasound stations are shown as white triangles. The explosion site Ichnya is marked with a white star.

5 SOURCES OF COHERENT NOISE AT CEEIN STATIONS

Detection performance of the CEEIN infrasound arrays is highly dependent on each station ambient noise conditions. This ambient noise comprises both incoherent wind noise and recurrent coherent infrasonic sources.

Station dependent factors that contribute to the noise include climate, station location relative to oceans, local topography, local noise sources, vegetation or snow cover at the sensor sites and configurations of sensors and wind-noise reduction filters (Ceranna *et al.* 2019). Typically, recurrent noise sources, both coherent and incoherent, can increase the background noise level and reduce array detection capability by decreasing the coherence between individual array elements (Bowman *et al.* 2005, 2009; Christie and Campus 2010). Whilst incoherent noise sources such as wind are not spatially correlated between array elements, coherent noise sources produce signals that are spatially correlated between array elements (Brown *et al.* 2014). Repeating or continuous coherent noise sources can produce false signal detections that affect the accuracy of signal identification with the infrasonic arrays (Woodward *et al.* 2005).

The ambient noise conditions are variable over time and among the CEEIN stations with seasonally consistent signals originating from various coherent noise sources both natural (microbaroms, volcanoes and storms) and anthropogenic, that is, industrial activity (refineries, power plants, dams and mining) or supersonic aircraft activity. The most well observed sources of noise with CEEIN arrays are the microbaroms (North and South Atlantic, Mediterranean Sea and Black Sea) that commonly produce coherent signals in the 0.1–0.8 Hz frequency band. Additional sources of repetitive coherent signals within the 0.5–5 Hz band, are related to Etna and local man-made activities.

Studying microbaroms helps the better understanding of the middle atmosphere dynamics (Hupe *et al.* 2019); signals from volcano eruptions contribute to global volcano monitoring systems. Identifying coherent anthropogenic noise sources helps distinguishing these sources from other signals, and thus reduce the false alarm rate when forming events.

We present the station detection capability plots for year 2020 obtained for IPLOR, BURARI, PSZI, PVCI, MAAG1, MAAG2 for trace velocities between 0.3 to 0.5 km s^{-1}. Progressive Multi-Channel Correlation (PMCC) detection algorithm (Cansi, 1995; Cansi and Le Pichon 2008; Mialle *et al.* 2019) was applied for data processing, that is, the Garcés (2013) detection algorithm embedded in the DASE toolkit (DTK) suite of software–for IPLOR, BURARI, PSZI and PVCI arrays and the PMCC 5.7 software used for MAAG1 and MAAG2 stations.

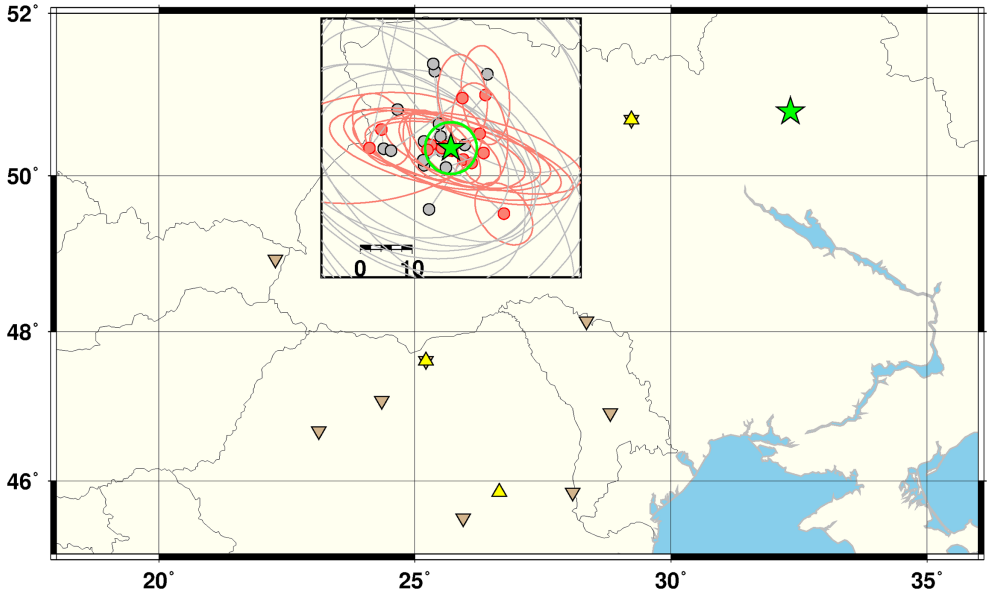

Figure 7. Event locations for Ichnya, Ukraine. Inverted triangles mark the seismic stations, yellow and beige triangles indicate CEEIN and IMS infrasound arrays that recorded the events. Green star indicates the ground truth location. The inset shows the enlarged vicinity of the GT locations. Red and grey circles indicate the CEEIN and IDC solutions, and grey and red lines show the corresponding error ellipses, respectively. The green circle is the 5 km radius around the GT site.

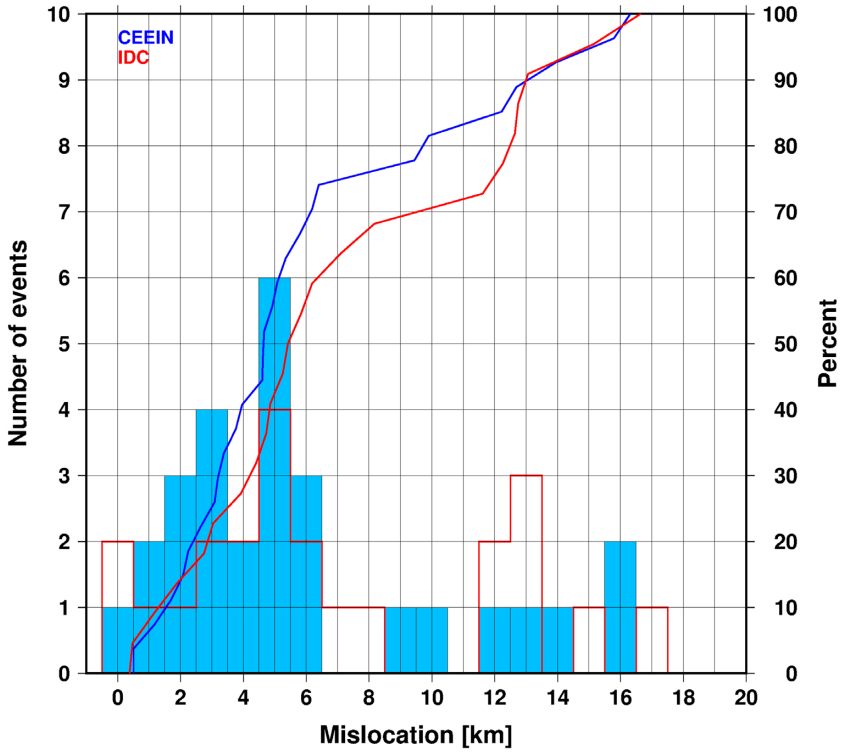

Figure 8. Histogram and cumulative distribution of mislocation of ground truth explosions by the IDC (red) and CEEIN (blue) seismo-acoustic event locations. The inclusion of CEEIN stations improves location accuracy.

Fig. 9 shows the PMCC detections of coherent noise for the CEEIN infrasound arrays, starting from the westernmost station PVCI to the easternmost station, MAAG1. The diagrams were plotted using DTK-DIVA visualization part of the DTK package. We identified the major sources of coherent noise as:

(i) Microbaroms (North and South Atlantic, Black Sea, Mediterranean Sea)

(ii) Volcano eruptions (Etna)

(iii) Gas flares at oil refineries (Romania, Bulgaria, Serbia, Hungary, Austria)

(iv) Thermal Power Plants (TPPs) (Hungary, Czechia)

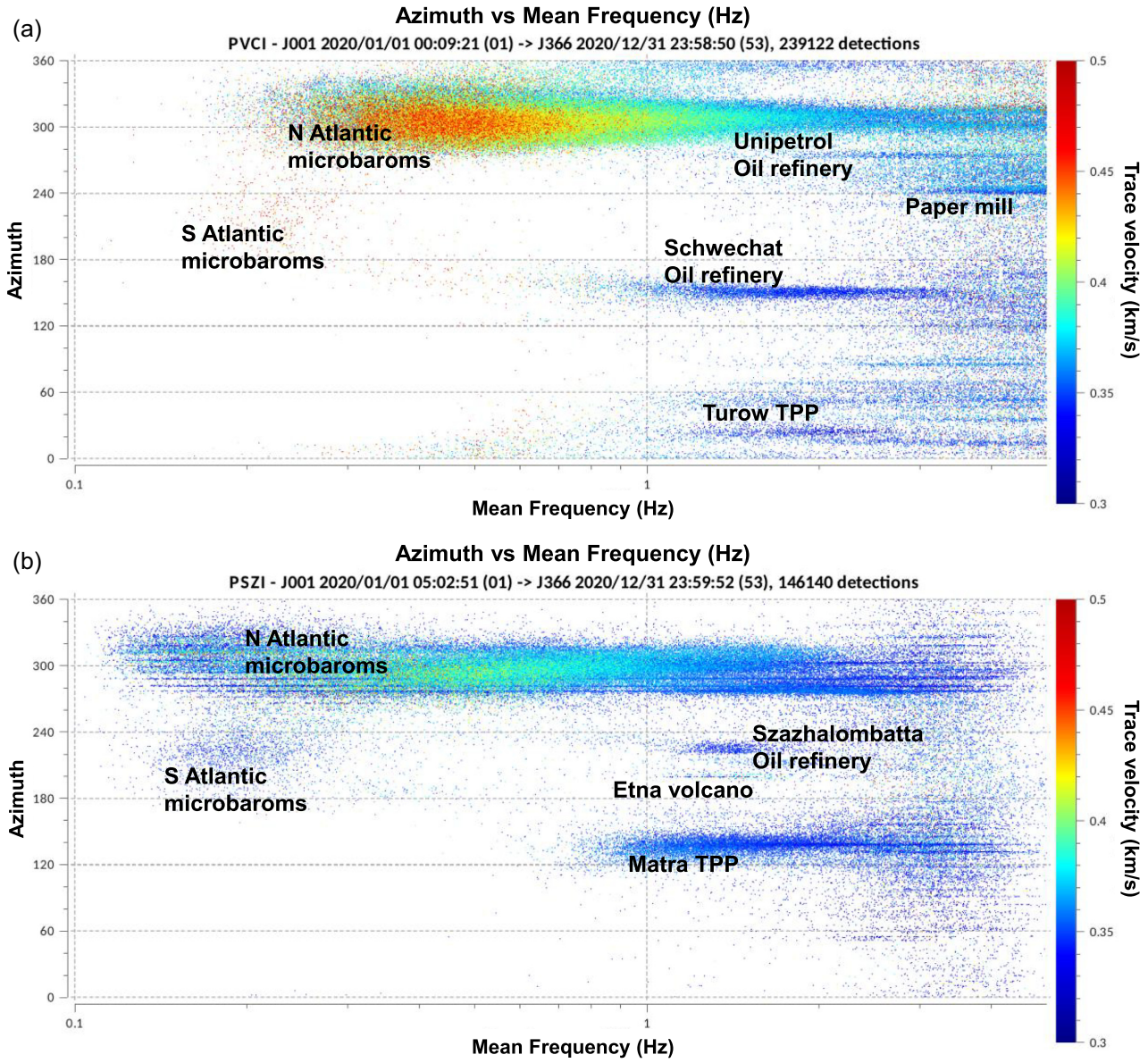

Figure 9. PMCC detection results at (a) PVCI, (b) PSZI, (c) BURAR, (d) IPLOR, (e) MAAG2 and (f) MAAG1 arrays. Mean frequency/backazimuth/trace velocity scatter plot. The main sources of coherent noise are indicated in the figures.

(v) Water discharges into the dams at Hydroelectric Power Plants (HEPPs)

All CEEIN stations record the microbaroms originated in the North Atlantic, but only the westernmost arrays see the South Atlantic microbaroms. The southernmost IPLOR sees both the Black Sea and Mediterranean Sea microbaroms. Each array records slightly different coherent anthropogenic noise sources.

6 DISCUSSION AND CONCLUSIONS

Infrasound azimuth observations are now routinely used in locating and identifying quarry blast and mine explosions in the region (Czanik *et al.* 2021; Ghica *et al.* 2016). For instance, since the PSZI infrasound array has begun operations in mid-2017, the percentage of events identified as quarry blasts in Hungary increased from 25–35 per cent to 70 per cent (Bondár *et al.* 2021). Despite the large number of quarry blasts detected by CEEIN stations, only a few are detected by more than one infrasound arrays. These (Bad Deutsch in Austria and Thetchea, in Romania) are listed in the CEEIN Bulletin.

Large earthquakes may also generate infrasound signals. The CEEIN bulletin contains two such events, the 2019 November 26 M6.4, Durres, Albania and the 2020 December 29 M6.4 Petrinja, Croatia.

Šindelářová *et al.* (2021) reported on the post-tropical storm Ophelia using CEEIN infrasound arrays, and Pásztor *et al.* (2021) and Rusz *et al.* (2021) demonstrated the use of infrasound stations in detecting lightnings and tracking regional storms.

North Sea sonic booms are frequently detected by European infrasound stations. The signals originate from supersonic aircraft flights above the North Sea. The region is well covered by infrasound arrays in Germany, in France, and in Netherlands. Nevertheless, the CEEIN stations can contribute to observations of the North Sea

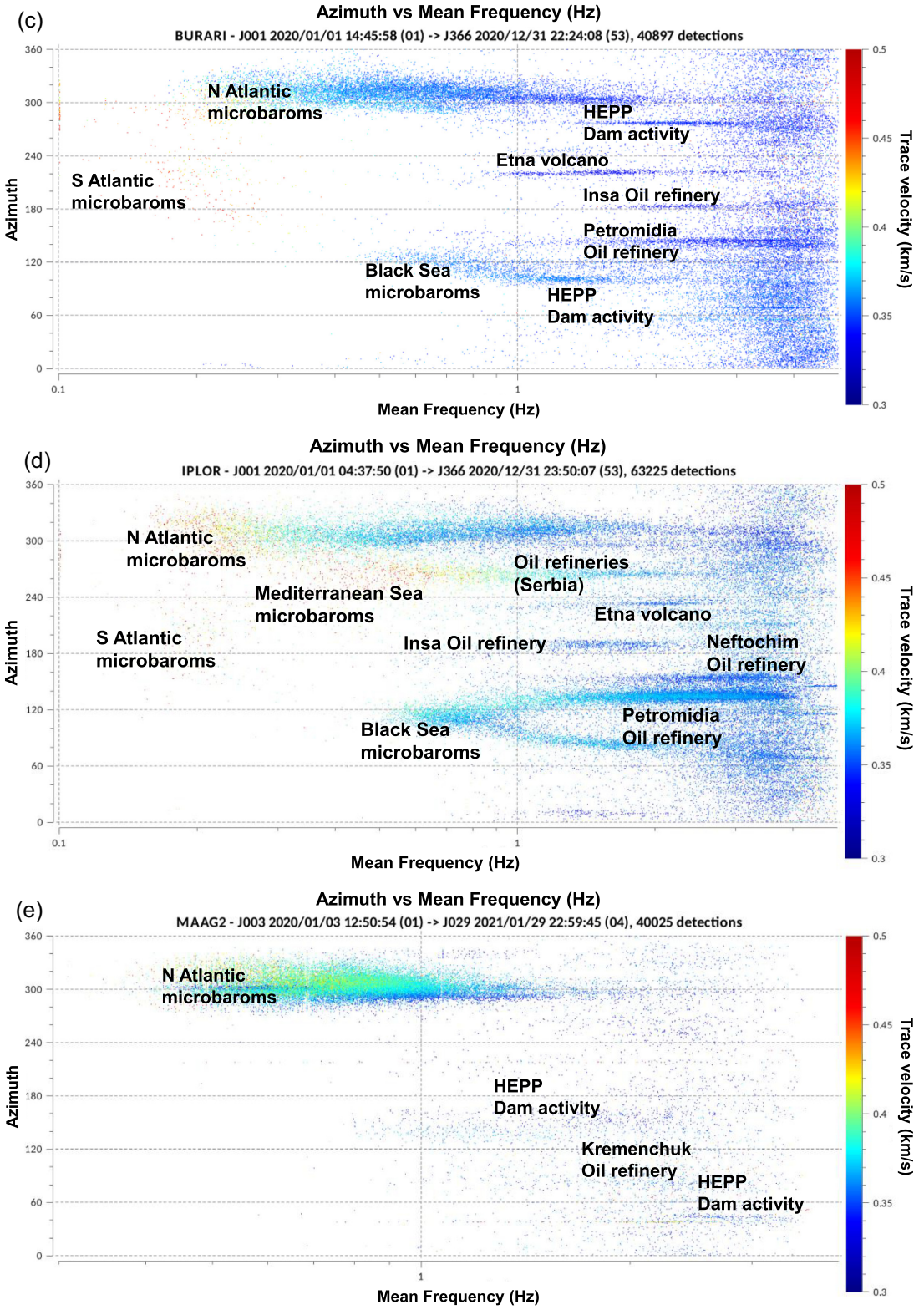

Figure 9. Continued.

sonic booms, particularly when infrasound detections in western Europe are deteriorated by high wind noise. The PSZI, IPLOR and BURAR infrasound arrays regularly report North Sea sonic booms. The stations are usually influenced by different weather systems than stations in western Europe. Thus, they can benefit from calm conditions while western European stations experience wind storms.

The dense network of infrasound station in Central and Eastern Europe enables detailed monitoring of the Aegean Sea region. The

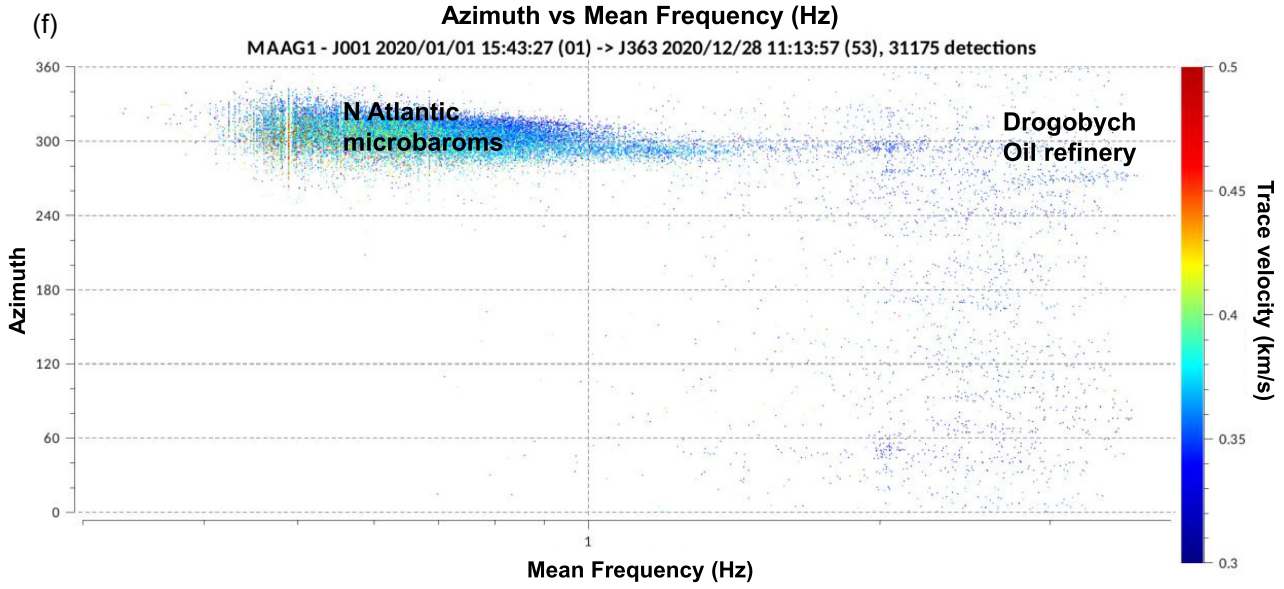

Figure 9. Continued.

good visibility of the Aegean region in all seasons is possible due to a convenient distribution of the CEEIN stations—some of the stations are located to the north-west and some are located to the north-east from the region of interest. Indeed, CEEIN stations frequently observe sonic booms in the Aegean region, even those not reported in the CTBTO LEBs. CEEIN can help not only to close the gap in detections, but also to locate events that would not be possible using IMS stations alone. Because of their favourable position to see the Eastern Mediterranean and the Black Sea, especially during the summer months, CEEIN stations also record microbaroms from the Black Sea. The knowledge of infrasound-producing sources within the region increases the capability to associate the detections to the true events versus coherent noise sources.

The observation results and event detections by CEEIN in 2017–2020 match with the predicted improvement of detection capability of infrasound network in Europe after CEEIN stations were included in the detections. The detection capability model expects significant reduction of detectable threshold amplitudes in the region between 25° and 55°N and between 15° and 35°E. CEEIN arrays close the gap in infrasound station coverage in Central and Eastern Europe. They not only reduce the detection capability threshold of the European infrasound network, but also add new detection capability in the Aegean region and Eastern Europe. Thus, CEEIN represents potentially significant contribution to infrasound monitoring and atmospheric studies in Europe. In the future we plan to comply with the latest IMS specifications for the existing and planned CEEIN infrasound arrays, most notably, to increase the number of sensors to improve the array geometry, aperture and the array transfer function.

ACKNOWLEDGMENTS

We thank Antoine Turquet and an anonymous reviewer for their comments that help to improve the paper. This work was supported by the National Research, Development and Innovation Fund (K128152), Hungary; the Czech Academy of Sciences and Hungarian Academy of Sciences mobility project (MTA-19-01 and NKM2018-10).

DATA AVAILABILITY

CEEIN waveform data from PSZI (doi:10.14470/UA114590), BURAR and IPLOR (doi:10.7914/SN/RO) are already available at the GEOFON and NIEP EIDA nodes, respectively. Waveforms from the rest of the CEEIN stations, PVCI (doi:10.7914/SN/C9), ISCO (doi:10.7914/SN/OE) and MAAG1, MAAG2 and GRD1 (doi:10.7914/SN/UD) shall be archived at the NIEP EIDA node from 2022 January 01. We used the CTBTO NDC-in-a-Box software (SeisComp3, DTK-PMCC, DTK-Diva) distributed by the Comprehensive Nuclear-Test-Ban Treaty Organization among the State Parties. The open-source iLoc can be downloaded from the IRIS software repository, https://seiscode.iris.washington.edu/projects/iloc.

REFERENCES

Begnaud, M. L., Anderson, D. N., Myers, S. C., Young, B., Hipp, J. R. & Phillips, W. S., 2021. Updates to the Regional Seismic Travel Time (RSTT) Model: 2. Path-dependent travel-time uncertainty, *Pure appl. Geophys,* **178,** 313–339.

Begnaud, M. L., Myers, S. C., Young, B., Hipp, J. R., Dodge, D. & Phillips, W. S., 2020. Updates to the Regional Seismic Travel Time (RSTT) Model: 1. Tomography, *Pure appl. Geophys.* **178,** 2475–2498.

Blanc, E. *et al.*, 2018. Toward an improved representation of middle atmospheric dynamics thanks to the ARISE project, *Surv. Geophys*. **39,** 171–225.

Bondár, I. P., Mónus, C., Czanik, M., Kiszely, Z. & Gráczer, Z., Wéber, AlpArrayWorking Group, 2018. Relocation of seismicity in the Pannonian Basin using a global 3D velocity model, *Seismol. Res. Lett.,* **89,** 2284–2293,.

Bondár, I., Czanik, C., Czecze, B., Kalmár, D., Kiszely, M., Mónus, P. & Süle, B., 2021. in *Hungarian Seismo-Acoustic Bulletin 2020,* ed. Bondár, I., ISSN: 2676-7902, CSFK GGI Kövesligethy Radó Szeizmológiai Obszervatórium, Budapest.

Bondár, I. & McLaughlin, K., 2009. Seismic location bias and uncertainty in the presence of correlated and non-Gaussian travel-time errors, *Bull. seism. Soc. Am.,* **99,** 172–193..

Bondár, I. & Storchak, D., 2011. Improved location procedures at the International Seismological Centre, *Geophys. J. Int.,* **186,** 1220–1244.

Bowman, J. R., Baker, G. E. & Bahavar, M., 2005. Ambient infrasound noise, *Geophys. Res. Lett.,* **32,** L09803.

Bowman, J. R., Shields, G. & O'Brien, M. S., 2009. Infrasound station ambient noise estimates and models 2003–2006 (Erratum), *Infrasound Technology Workshop, Brasilia, Brazil*.

Brown, D., Ceranna, L., Prior, M., Mialle, P. & Le Bras, R., 2014. The IDC seismic, hydroacoustic and infrasound global low and high noise models, *Pure appl. Geophys.,* **171,** 361–375.

Cansi, Y., 1995. An automatic seismic event processing for detection and location: the P.M.C.C. Method, *Geophys. Res. Lett.,* **22,** 1021–1024.

Cansi, Y. & Le Pichon, A., 2008. Infrasound event detection using the progressive Multi-Channel correlation algorithm, in *Handbook of Signal Processing in Acoustics,* eds. Havelock, D., Kuwano, S. & Vorlnder, M., Springer, New York, NY..

Ceranna, L., Matoza, R., Hupe, P., Le Pichon, A. & Landès, M., 2019. Systematic array processing of a decade of Global IMS infrasound data, in *Infrasound Monitoring for Atmospheric Studies,* pp. 471–482, eds. Le Pichon, A., Blanc, E. & Hauchecorne, A., Springer, Cham.

Che, I. Y., Park, J., Kim, T. S., Hayward, C. & Stump, B., 2019. On the use of a dense network of seismo-acoustic arrays for near regional environmental monitoring, in *Infrasound Monitoring for Atmospheric Studies,* 2nd ed., pp. 409–448, eds. Le Pichon, A., Blanc, E. & Hauchecorne, A., Springer, Cham.

Christie, D. R. & Campus, P., 2010. The IMS Infrasound Network: Design and establishment of infrasound stations, in *Infrasound Monitoring for Atmospheric Studies,* pp. 29–75, eds. Le Pichon, A., Blanc, E. & Hauchecorne, A., Springer, Dordrecht.

Chum, J., Liu, J.-Y., Podolská, K. & Šindelářová, T., 2018. Infrasound in the ionosphere from earthquakes and typhoons, *J. Atmos. Sol. Terr. Phys.,* **171,** 72–82.

Chum, J., Podolská, K., Rusz, J., Baše, J. & Tedoradze, N., 2021. Statistical investigation of gravity wave characteristics in the ionosphere, *Earth Planets Space,* **73,** 60.

Collins, D., 1993. A split-step Pade solution for parabolic equation mehod, *J. acoust. Soc. Am.,* **93,** 1793–1742.

Czanik, C. *et al.*, 2018. The Central and Eastern European Infrasound Network, *Infrasound Technology Workshop,* Vienna, Austria.

Czanik, C., Kiszely, M., Mónus, P., Süle, B. & Bondár, I., 2021. Identification of quarry blasts aided by infrasound data, *Pure appl. Geophys.,* **178,** 2287–2300.

Fuchs, F., Schneider, F. M., Kolinsky, P., Serafin, S. & Bokelmann, G., 2019. Rich observations of local and regional infrasound phases made by the AlpArray seismic network after refinery explosion, *Sci. Rep.,* **9,** 13027.

Gainville, O., Blanc-Benon, P., Blanc, E., Roche, R., Millet, C., Le Piver, F., Despres, B. & Piserchia, P. F., 2010. Misty picture: a unique experiment for the interpretation of the infrasound propagation from large explosive sources, in *Infrasound Monitoring for Atmospheric Studies,* eds. Le Pichon, A., Blanc, E. & Hauchecorne, A., Springer Science Dordrecht, pp. 575–598.

Garcés, M. A., 2013. On infrasound standards, part 1: time, frequency, and energy scaling, *InfraMatics,* **2,** 13–35.

Ghica, D. V., Grecu, B., Popa, M. & Radulian, M., 2016. Identification of blasting sources in the Dobrogea seismogenic region, Romania using seismo-acoustic signals, *Phys. Chem. Earth,* **95,** 125–134.

Gibbons, S., Kværna, T. & Näsholm, P., 2019. Characterization of the infrasonic wavefield from repeating seismo-acoustic events, in *Infrasound Monitoring for Atmospheric Studies,* 2nd ed., pp. 387–407, eds. Le Pichon, A., Blanc, E. & Hauchecorne, A., Springer, Cham.

Green, D. N. & Bowers, D., 2010. Estimating the detection capability of the International Monitoring System infrasound network, *J. geophys. Res.,* **115,** D18116.

Green, D. N., Vergoz, J., Gibson, R., Le Pichon, A. & Ceranna, L., 2011. Infrasound radiated by the Gerdec and Chelopechene explosions: propagation along unexpected paths, *Geophys. J. Int.,* **185,** 890–910.

Hupe, P., Ceranna, L., Pilger, C., de Carlo, M., Le Pichon, A., Kaifler, B. & Rapp, M., 2019. Assessing middle atmosphere weather models using infrasound detections from microbaroms, *Geophys. J. Int.,* **216,** 1761–1767.

International Seismological Centre, 2021. On-line bulletin, *International Seismological Centre,* Thatcham, United Kingdom, Available at:http://www.isc.ac.uk.

IRIS DMC, 2012, Data Services Products: infrasound TA infrasound data products, Available at: https://ds.iris.edu/ds/products/infrasound/.

Koch, K. & Pilger, C., 2020. A comprehensive study of infrasound signals detected from the Ingolstadt, Germany, explosion of 1 September 2018, *Pure appl. Geophys,* **177,** 4229–4245.

Koch, K., Pilger, C., Czanik, C. & Bondár, I., 2020. The 12 December 2017 Baumgarten Gas Hub Explosion: a case study on understanding the occurrence of a large infrasound azimuth residual and a lack of seismic observations, *Pure appl. Geophys.,* **177,** 4957–4970.

Laštovička, J. & Chum, J., 2017. A review of results of the international ionospheric Doppler sounder network, *Adv. Space Res.,* **60,** 1629–1643.

Le Pichon, A., Ceranna, L. & Vergoz, J., 2012. Incorporating numerical modeling into estimates of the detection capability of the IMS infrasound network, *J. geophys. Res.,* **117,** D05121.

Le Pichon, A., Vergoz, J., Blanc, E., Guilbert, J., Ceranna, L., Evers, L. & Brachet, N., 2009. Assessing the performance of the International Monitoring System's infrasound network: geographical coverage and temporal variabilities, *J. geophys. Res.,* **114,** D08112.

Marty, J., 2019. The IMS Network: current status and technological developments, in *Infrasound Monitoring for Atmospheric Studies,* 2nd ed., pp. 3–62, eds. Le Pichon, A, Blanc, E. & Hauchecorne, A., Springer, Cham.

Mialle, P., Brown, D. & Arora, N., and colleagues from IDC, 2019. Advances in operational processing at the International Data Centre, in *Infrasound Monitoring for Atmospheric Studies,* 2nd ed., pp. 209–248, eds. Le Pichon, A., Blanc, E. & Hauchecorne, A., Springer Cham.

Myers, S. C. *et al.*., 2010. A crust and upper-mantle model for Eurasia and North Africa for Pn travel-time calculation, *Bull. seism. Soc. Am.,* **100,** 640–656.

Pásztor, M., Czanik, C., Chum, J., Šindelářová, T. & Bondár, I., 2021. Identifying and tracking regional storms with infrasound data, *CTBTO Science and Technology Conference,* P2.3–585, Vienna, Austria, Available at: https://conferences.ctbto.org/event/7/book-of-abstracts.pdf.

Pilger, C. *et al.*, 2018. The European infrasound bulletin, *Pure appl. Geophys.,* **175,** 3619–3638.

Rusz, J., Chum, J. & Baše, J., 2021. Locating thunder source using a large-aperture micro-barometer array, *Front. Earth Sci*., **9,** 614820.

Schneider, F. M., Fuchs, F., Kolinsky, P., Caffagni, E., Serafin, S., Dorninger, M. & Bokelmann, G., AlpArray Working Group, 2018. Seismo-acoustic signals of the Baumgarten (Austria) gas explosion detected by the AlpArray seismic network, *Earth Planet. Sci. Lett.,* **502,** 104–114.

Šindelářová, T. *et al.*, 2018. Towards a regional infrasound network in Central and Eastern Europe in support of ARISE, *Atmospheric Research InfraStructure in Europe Workshop,* Hamburg, Germany.

Šindelářová, T. *et al.*, 2021. Infrasound signature of the post-tropical storm Ophelia at the Central and Eastern European Infrasound Network, *J. Atm. Solar-Terr. Phys.,* **217,** 105603..

Šindelářová, T., Burešová, D. & Chum, J., 2009. Observations of acoustic-gravity waves in the ionosphere generated by severe tropospheric weather, *Stud. Geophys. Geod.,* **53,** 403–418.

Sutherland, L. C. & Bass, H. E., 2004. Atmospheric absorption in the atmosphere up to 160 km, *J. acoust. Soc. Am.,* **115,** 012–1032.

Szuberla, C. A. L. & Olson, J. V., 2004. Uncertainties associated with parameter estimation in atmospheric infrasound arrays, *J. acoust. Soc. Am,* **115,** 253.

Trabant, C., Hutko, A. R., Bahavar, M., Karstens, R., Ahern, T. & Aster, R., 2012, Data products at the IRIS DMC: stepping stones for research and other applications, *Seismol. Res. Lett.,* **83,** 846–854.

Varypaev, A., Volosov, S., Konstantinovskaya, N., Nesterkina, M., Kharlamov, V. & Rybnov, Y., 2019. Seismo-acoustic effects of the lipetsk bolide 21.06.2018, in *Trigger Effects in Geosystems. Springer Proceedings in Earth and Environmental Sciences,* eds. Kocharyan, G. & Lyakhov, A., Springer, Cham.

Walker, K. T., Shelby, R., Hedlin, M. A., de Groot-Hedlin, C. & Vernon, F., 2011. Western u.s. infrasonic catalog: Illuminating infrasonic hot spots with the usarray, *J. geophys. Res.,* **116,** B12305.

Weber, B., Bondár, I., Rößler, D. & Becker, J., 2019. SeisComP3 iLoc integration applied to array processing, T3.5-P54, *CTBTO Science and Technology Conference,* p.187, Vienna, Austria.

Woodward, R., Israelsson, H., Bondár, I., Mclaughlin, K., Bowman, J. R. & Bass, H., 2005. Understanding wind-generated infrasound noise, *Proceedings of the 27th Seismic Research Review: Ground-Based Nuclear Explosion Monitoring Technologies*. Palm Springs, CA, September 20-22, 2005, pp. 866–875.

SUPPORTING INFORMATION

Supplementary data are available at *GJI* online.

Please note: Oxford University Press is not responsible for the content or functionality of any supporting materials supplied by the authors. Any queries (other than missing material) should be directed to the corresponding author for the article.